Trivalent Actinide Uptake by Iron (Hydr)oxides

Nicolas Finck,*[,†] Sorin Nedel,[‡,∥] Knud Dideriksen,[‡] and Michel L. Schlegel[§]

[†]Institute for Nuclear Waste Disposal (INE), Karlsruhe Institute of Technology (KIT), P.O. Box 3640, D 76021 Karlsruhe, Germany
[‡]Nano Science Center, Department of Chemistry, University of Copenhagen, Universitetsparken 5, DK 2100 Copenhagen, Denmark
[§]CEA, DEN/DPC/SEARS/LISL, Building 391, F 91191 Gif sur Yvette, France

ABSTRACT: The retention of Am(III) by coprecipitation with or adsorption onto preformed magnetite was investigated by X ray diffraction (XRD), solution chemistry, and X ray absorption spectros copy (XAS). In the coprecipitation experiment, XAS data indicated the presence of seven O atoms at 2.44(1) Å, and can be explained by an Am incorporation at Fe structural sites at the magnetite surface. Next nearest Fe were detected at distances suggesting that Am and Fe polyhedra share corners in geometries ranging from bent to close to linear Am−O−Fe bonds. After aging for two years, the coordination number and the distance to the first O shell significantly decreased, and atomic shells were detected at higher distances. These data suggest a structural reorganization and an increase in structural order around sorbed Am. Upon contact with preformed Fe_3O_4, Am(III) forms surface complexes with cosorbed Fe at the surface of magnetite, a possible consequence of the high concentration of dissolved Fe. In a separate experiment, chloride green rust (GR) was synthesized in the presence of Am(III), and subsequently converted to $Fe(OH)_2$(s) intermixed with magnetite. XAS data indicated that the actinide is successively located first at octahedral brucite like sites in the GR precursor, then in $Fe(OH)_2$(s), an environment markedly distinct from that of Am(III) in Fe_3O_4. The findings indicate that the magnetite formation pathway dictates the magnitude of Am(III) incorporation within this solid.

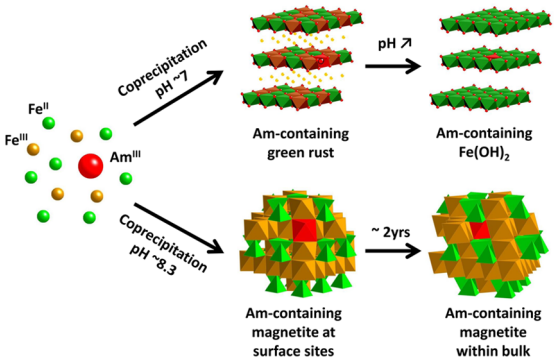

■ INTRODUCTION

Deep geological disposal is considered a prime solution for the safe management of high level nuclear waste (HLW), such as spent nuclear fuel and waste from reprocessing. In such deep facilities, the HLW will be confined in steel canisters which are foreseen to be surrounded successively by man made (engineered) and natural (host rock) barriers (an overview of European concepts can be found in[1]). In this multibarrier system, the host rock and the engineered barrier are both expected to hinder groundwater flow to the waste packages. However, these barriers are expected to lose their confining properties over geological time scales and the intrusion of groundwater will result in corrosion of steel canister containing the HLW. Corrosion studies performed over time scales of months to years[2−9] have shown that steel corroded in the presence of clay or clay porewater produces Fe(II) bearing phases such as green rust or magnetite (Fe_3O_4).[10]

The classical mechanism of magnetite formation during anaerobic steel corrosion at elevated temperatures follows a two step process. In a first step, ferrous hydroxide and hydrogen are produced by water reduction and iron oxidation. Subsequently, $Fe(OH)_2$(s) is oxidized by water to form hydrogen and the thermodynamically more stable magnetite (Schikorr reaction).[11] Additionally, partial oxidation of Fe $(OH)_2$(s) (e.g., during an oxic transient) can also form green rust (GR), which belongs to the family of Fe(II)−Fe(III) layered double hydroxides.[12] Indeed, GRs have been identified on corroding iron and steel (e.g., refs 10, 13, and 14) and are known to be transient compounds between metallic iron and final corrosion products.

Secondary Fe phases formed by steel corrosion can form an additional barrier to radionuclide (RN) migration. Specifically, RN released upon waste matrix alteration can be either retained onto preformed corrosion products or incorporated within the bulk of these phases.[15] Furthermore, hydrogen evolution upon iron oxidation will impose strongly reducing conditions, possibly reducing RN (such as the long lived and radiotoxic actinides, including americium) to lower oxidation state(s).[15] Information on the molecular scale retention process of reduced actinides species by Fe(II) bearing corrosion phases (e.g., GR, Fe_3O_4) is thus of prime importance for safety performance assessment of a HLW repository.

The interaction of trivalent lanthanides (Ln(III)), used as surrogates for the actinides, with GR or Fe_3O_4 has been investigated in previous studies. For example, the biotical and abiotical preparation of magnetite in the presence of various trivalent lanthanides has been reported[16−19] and in all studies the substitution for octahedral Fe(III) was assumed based on measured (e.g., physical and magnetic) properties. The fate of Ce(III) during the preparation of GR and magnetite from preformed ferrihydrite has been investigated by Nedel et al.[20]

Table 1. Chemical Conditions in the Experiments[a]

sample	$[Fe(II)]_i$ mol/L	$[Fe(III)]_i$ mol/L	$[Am(III)]_i$ mol/L	pH_f	$E_{h,f}$ mV vs S.H.E.	$[Fe]_f$ mol/L	$[Am(III)]_f$ mol/L	solid mass concentration (g/L)	Am content (g/g)
AmCopGR	43.3×10^{-3}	6.3×10^{-3}	32×10^{-6}	7.00	333	16×10^{-3}	4.3×10^{-7}	3.6	2.1×10^{-3}
AmCopGRtrans				11.00	518	6.2×10^{-7}	2.1×10^{-9}	2.1	2.1×10^{-3}
AmCopMag	16.5×10^{-3}	33.3×10^{-3}	33×10^{-6}	8.25	295	3.6×10^{-7}	3×10^{-10}	3.8	2.0×10^{-3}
AmAdsMag			20×10^{-6}	5.70	23	1.4×10^{-3}	11×10^{-9}	2.0	2.4×10^{-3}
AmCopMagAged	16.6×10^{-3}	33.3×10^{-3}	34×10^{-6}	(12.25) 12.50	(455) 222	4.1×10^{-7}	2×10^{-10}	3.9	2.1×10^{-3}

[a]Subscript i denotes initial conditions, subscript f denotes final conditions, and values in parentheses for sample AmCopMagAged refer to values before aging. Uncertainties are estimated to ±0.1 unit on pH values, ± 30 mV on E_h values and ±10 15% on the concentrations. (S.H.E.: standard hydrogen electrode).

Ce(III) initially retained by ferrihydrite was only partially released upon phase transformation to magnetite but was quantitatively released upon transformation of ferrihydrite to GR. Separately, studies indicate that preformed magnetite has a high affinity for sorption of Ln(III).[21−23] However, no study reported structural data by directly probing the retained Ln(III) species.

Only very few investigations on the retention by magnetite of RN such as trivalent[24−26] or tetravalent[27,28] actinides or Tc[29] have been reported so far. In contrast, a larger number of investigations on the retention by preformed magnetite of actinides in higher oxidation states, such as U(VI),[30−35] Np(V)[36,37] or Pu(V)[25,38] have been published. Interestingly, the actinides were generally retained by reductive immobiliza tion at the magnetite surface, correlating with a partial Fe(II) oxidation. A similar immobilization mechanism has been shown to operate for Tc(VII),[39] U(VI)[40,41] or Np(V)[42,43] contacting preformed GR.

The incorporation of RN within the bulk structure of corrosion phases represents another effective immobilization mechanism. Because magnetite and GR both have octahedral Fe(III) sites, a homovalent substitution of trivalent actinides for octahedral Fe atoms in these solids can be expected. However, the substitution may be hindered due to size mismatch between 6 fold oxygen coordinated Fe(III) (r^{VI}(Fe(III)) = 0.65 Å) or Fe(II) (r^{VI}(Fe(II)) = 0.78 Å) and trivalent transuranic actinides (e.g., r^{VI}(Pu(III)) = 1.00 Å, r^{VI}(Am(III)) = 0.98 Å, r^{VI}(*Cm*(III)) = 0.97 Å).[44] Yet, recent studies on the incorporation of Am(III) at octahedral sites in brucite and sheet silicates,[45] as well as in calcite,[46] suggest that such an incorporation, although limited, is actually possible.

In this study, we investigated the incorporation of Am(III) in magnetite, either by direct precipitation with aqueous Fe(II) and Fe(III), or by incorporation in a GR precursor followed by conversion of this solid. Separately, Am(III) was contacted with preformed magnetite and used as reference compound. X ray diffraction (XRD) and scanning electron microscopy (SEM) were used to characterize the solid samples, and the Am(III) binding environment was deciphered by probing the Am L_3 edge by X ray absorption spectroscopy (XAS). The purpose of this study is to investigate on the structural incorporation of Am(III) within iron (hydr)oxides that are expected to form upon steel canister corrosion in deep HLW disposal sites.

■ MATERIALS AND METHODS

Samples and Reference Compounds Preparation. All samples were prepared with ultrapure water (18.2 MΩ·cm, Milli Q system, Millipore) and reagents of ACS grade or higher. To avoid oxidation by air, all samples were prepared and handled in an Ar filled glovebox (<1 ppmv O_2) and all measurements (XRD, XAS, SEM) were performed under anoxic conditions. The Fe(II) and Fe(III) sources were chloride salts and the Am(III) stock solution contained 15 mmol/L ^{243}Am (~27 MBq/mL) in 1 M HCl. This nuclide is an α emitter (half life of 7370 years), and so all operations were carried out in radiochemical laboratories equipped for handling this isotope. pH was measured with a combined electrode that was calibrated every day, and adjusted, when necessary, by using HCl or NaOH prepared in the glovebox. E_h values were measured using a Pt electrode. Suspensions were stirred during pH and E_h measurements, values are indicated in Table 1.

Chloride GR formed in the presence of Am(III) (sample AmCopGR) was prepared by addition of NaOH to a stirred solution containing Fe(II) and Fe(III) (Fe(II):Fe(III) molar ratio of ~7:1) spiked with ^{243}Am at concentrations indicated in Table 1. After 2 days, pH and E_h values were measured and 10 mL of the suspension were centrifuged in the glovebox for 10 min at 6500 rpm. The supernatant was removed and replaced by ultrapure water (mass/volume = 2.1 g/L) and the pH raised by addition of NaOH while stirring to induce transformation into magnetite (sample AmCopGRtrans). pH and E_h values were measured after 2 days of reaction. Separately, magnetite was prepared in the presence of Am(III) (sample AmCopMag) similarly to AmCopGR but with a Fe(II):Fe(III) molar ratio of 1:2 (Table 1). To probe the fate of Am during aging of magnetite, sample AmCopMagAged was prepared by dropwise addition of a solution containing Fe(II) and Fe(III) spiked with ^{243}Am to 100 mL of 0.038 mol/L NaOH under stirring. pH and E_h values were measured after 1 day, and the suspension was then left to age in the glovebox for two years. Finally, Am(III) ions were exposed to preformed magnetite in suspension to form sample AmAdsMag. For that sample, pure magnetite (sample Mag) was first prepared by addition of NaOH to a stirred solution containing Fe(II) and Fe(III) (Fe(II):Fe(III) molar ratio of 1:2). After 1 day, the suspension was centrifuged, the supernatant removed and Mag dispersed in 0.1 mol/L NaCl. Americium was then added to this suspension under stirring and allowed to react for 2 days before pH and E_h measurements. Assuming as a first approximation a specific surface area of 15 m^2/g and a surface site density of 5 sites/nm^2, the surface coverage was on the order of 10% in AmAdsMag. A portion of each suspension was also ultra centrifuged for 1 h at 694,000 *g* (Beckman XL 90) and the concentrations of dissolved Fe and Am in the supernatants ($[Fe]_f$ and $[Am(III)]_f$, respectively, in Table 1) were determined by high resolution ICP MS (Thermo Element XR).

Two samples were used as model compounds for XAS: a solution containing 0.011 mol/L ^{243}Am in 1 M HCl (sample $Am(III)_{aq}$) and an $Am(OH)_3(s)$ precipitate (sample AmHy

Table 2. Quantitative EXAFS Analysis of Samples and Reference Compounds

sample	FT range[a] [Å^{-1}]	Fit range[b] [Å]	shell	N	R [Å]	σ^2 [Å^2]	ΔE_0 [eV]	R_f
$Am(III)_{aq}$	3.2 10.3	1.7 2.6	O_1	9.0(5)	2.47(2)	0.007(2)	1.3	0.003
AmHydrox	3.4 10.1	1.6 4.2	O_1	5.7(10)	2.39(2)	0.009(3)	0.7	0.005
			O_2	1.6(5)	3.36(6)	0.007(8)		
			Am_1	1.7(11)	3.76(6)	0.008(4)		
			O_3	3.7(29)	4.36(8)	0.007(4)		
AmCopGR	3.3 9.1	1.6 4.2	O_1	6.5(4)	2.42(1)	0.007(1)	0.2	0.013
			Fe_1	1.6(4)	3.43(2)	0.006(3)		
			Fe_2	1.2(6)	4.02(4)	0.006(3)		
AmCopGRtrans	3.3 9.1	1.6 4.1	O_1	6.1(4)	2.43(1)	0.007(1)	1.4	0.010
			Fe_1	1.6(4)	3.47(2)	0.007(3)		
			Fe_2	1.6(5)	3.94(4)	0.007(3)		
AmCopMag	3.3 9.5	1.6 4.1	O_1	7.1(5)	2.44(1)	0.008(1)	0.4	0.015
			Fe_1	3.7(7)	3.45(2)	0.008(2)		
			Fe_2	1.6(5)	3.98(5)	0.008(2)		
AmCopMagAged	3.3 9.0	1.6 3.9	O_1	5.1(4)	2.39(2)	0.006(1)	1.7	0.018
			Fe_1	1.5(5)	3.40(3)	0.006(2)		
			O_2	1.0(5)	3.98(14)	0.006(2)		
AmAdsMag	3.2 9.4	1.6 3.9	O_1	8.8(5)	2.48(1)	0.009(1)	1.2	0.015
			Fe_1	5.5(7)	3.50(2)	0.007(2)		

[a]Fourier transformed range. [b]$R + \Delta R$ interval for the fit. N is the coordination number, R is the interatomic distance, σ^2 is the mean square displacement, ΔE_0 is the shift in ionization energy with E_0 threshold energy taken as maximum of the first derivative and R_f is the figure of merit of the fit as reported in.[45] The number in parentheses indicates the uncertainty.

drox). AmHydrox was prepared by addition of NaOH to a stirred acidic Am(III) solution (3.6×10^{-3} mol/L ^{243}Am) under air. This precipitate was washed several times with dilute NaOH and aged 5 h at 80 °C in 2 M NaOH. The resulting compound was centrifuged, washed several times, and measured as settled solid in suspension. AmHydrox had an X ray amorphous structure, as indicated from the absence of peak on the X ray diffractogram (data not shown).

Solid Phase Characterization. Solid phases were characterized by XRD and SEM. A small amount of sample slurry was allowed to dry on an airtight sample holder in the Ar filled glovebox and used to record XRD data on a D8 Advance (Cu Kα radiation) diffractometer (Bruker) equipped with an energy dispersive detector (Sol X). The phases were identified by comparison with the PDF 2 database. Information on the size and morphology of the powders was obtained by SEM with an environmental scanning electron microscope Quanta 650 FEG (FEI). Samples were prepared in the glovebox (slurry dried on holder), transported to the microscope under anoxic conditions and quickly positioned in the microscope to minimize the exposure time to air.

X-ray Absorption Spectroscopy. Information on the Am(III) local environment was provided by probing the Am L_3 edge by XAS at the INE Beamline[47] for actinide science at the synchrotron light source ANKA (Karlsruhe, Germany). The storage ring energy was 2.5 GeV and the ring current was 90–180 mA. The incident beam was monochromatized using a pair of Ge(422) crystals. Energy calibration was done by assigning the first inflection point of the Zr K edge of a Zr foil at 17998.0 eV and this reference was measured in parallel with all samples. Data were collected in fluorescence mode using a 5 element LEGe solid state detector (Canberra Eurisys). For XAS data collection, all samples were mounted within a double envelope container to meet safety regulations and keep anoxic conditions, using a setup described in Brendebach et al.[48] For each sample, five to six scans were recorded to improve the signal to noise ratio.

Data were analyzed following standard procedures by using Athena and Artemis interfaces to the Ifeffit software.[49] Extended X ray absorption fine structure (EXAFS) spectra ($\chi(k)$) were extracted from the raw data and Fourier transforms (FTs) were obtained from the $k^3 \times \chi(k)$ functions. The data were fit in the R space by using a combination of single scattering paths. For each coordination shell phase and amplitude functions were calculated separately with feff 8.4,[50] and the amplitude reduction factor was set to 0.82. The uncertainties on coordination numbers and bond distances are indicated in parentheses in Table 2. The fit quality was quantified by the R_f factor, as reported in,[45] representing the absolute misfit between theory and data.

RESULTS AND INTERPRETATION

Bulk Structure and Solution Chemistry. X ray diffractograms of all solid phases are presented in Figure 1 and scanning electron micrographs in Figure 2. Sample AmCopGR consists mainly of GR with typical hexagonal platelets of several hundred nanometers in size. Small amounts of magnetite were detected by XRD, most likely due to partial GR oxidation during sample measurement. Small amounts of soluble $FeCl_2 \bullet 2H_2O$ and NaCl were also detected, which had formed upon drying of unreacted Fe(II) and background salt. Analysis of the supernatant indicates that about one third of the Fe remained dissolved (Table 1). This corresponds almost exclusively to Fe(II) because the Fe(III) solubility at near neutral pH is very low in the absence of ligands. Based on the $[Fe]_f$ value, the Fe(II):Fe(III) molar ratio in the solid is about 4:1. This value is compatible with the reported maximal ratio in chloride GR[51] and probably results from the high Fe(II):Fe(III) ratio in the starting solution (Table 1). Analysis of the supernatant also indicates that more than 98% of Am is associated with the solid.

Sample AmCopGRtrans, obtained by transformation of AmCopGR, consists of large hexagonal platelets (up to several micrometers in size) covered by fine grained material (Figure

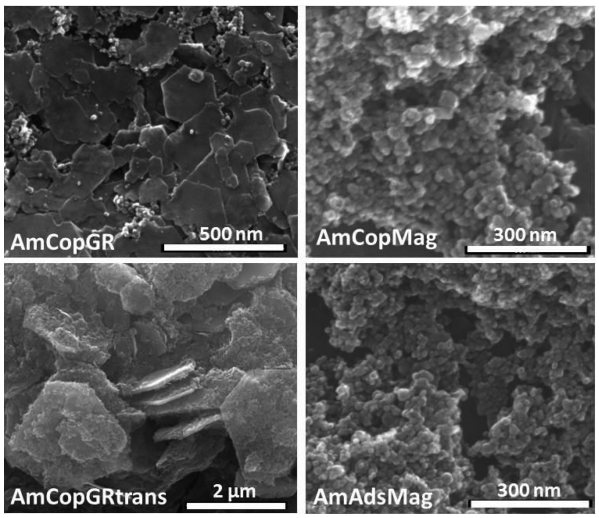

Figure 1. X ray diffractogram of samples AmCopGR, AmCopGRtrans, AmCopMag, and Mag (used as substrate in the adsorption experiment and reference magnetite powder), and reference data from the PDF 2 database. Detail on sample preparation is given in the text and chemical conditions of sample preparation are indicated in Table 1.

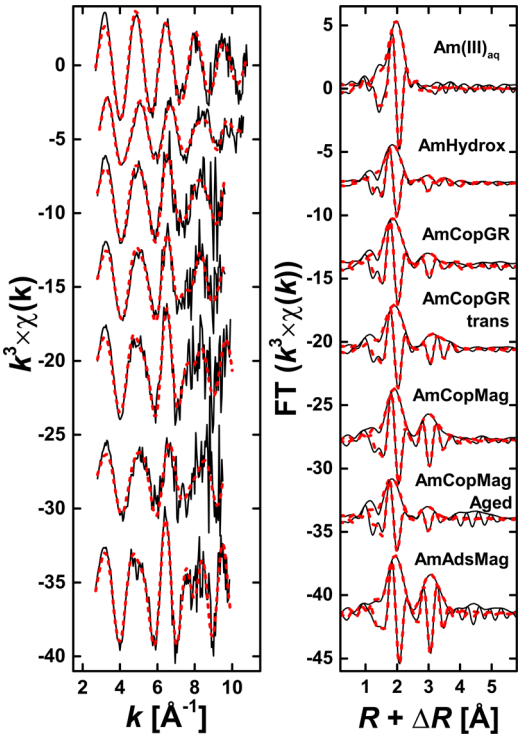

Figure 2. Scanning electron micrographs of samples AmCopGR, AmCopGRtrans, AmCopMag and AmAdsMag. Detail on sample preparation is given in the text and chemical conditions of sample preparation are indicated in Table 1.

2). XRD data indicate the presence of ferrous hydroxide (narrow peak) and magnetite (broad peaks) in this sample. Based on the crystal habit of these compounds, the platelets are identified as $Fe(OH)_2(s)$ and the fine grained material as magnetite. The formation of $Fe(OH)_2(s)$ and Fe_3O_4 by increasing the pH of a GR containing suspension corroborates earlier findings of Jolivet et al.[52] for sulfate GR. The $[Fe]_f$ and $[Am]_f$ values are very low (6.2×10^{-7} mol/L and 2.1×10^{-9} mol/L, respectively, Table 1), indicating almost no Am release during phase transformation. It is worth noting that in that sample, Am can possibly be bound to both $Fe(OH)_2(s)$ and Fe_3O_4. Very weak peaks in the XRD data at about 22, 35, and 40°2θ suggest the presence of trace amounts of an additional phase, possibly unreacted GR or goethite. However, given the weak intensity of the peaks, the amount of the phase is negligible.

Only fine grained material consisting of Fe_3O_4 could be detected in the magnetite directly precipitated in the presence of Am(III) (sample AmCopMag, Figures 1 and 2). The morphology and structure are identical to those of the magnetite substrate used in the adsorption experiment (Mag), indicating that Am(III) presence had no detectable influence on magnetite formation. Only trace amounts of Fe and Am could be detected in the supernatant (Table 1), indicating quantitative Am uptake by Fe_3O_4. Similarly, $[Fe]_f$ and $[Am]_f$ values for sample AmCopMagAged are very low and comparable to that measured for AmCopMag (Table 1). This result provides evidence that Am(III) was not released from the solid phase during sample aging. Finally, only trace amounts of Am could be detected in the AmAdsMag supernatant, but $[Fe]_f$ was rather high (1.4×10^{-3} mol/L). This high $[Fe]_f$ value could originate either from incomplete supernatant removal after synthesis of the magnetite substrate or from Fe(II) leaching from Fe_3O_4 under slightly acidic pH conditions.[53]

Local Chemical Environment of Am(III). The experimental and modeled EXAFS spectra of all samples, together with their FTs, are presented in Figure 3 and the fit results in

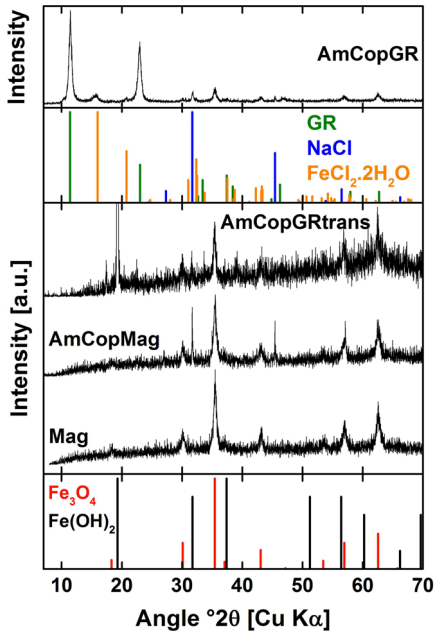

Figure 3. Experimental (solid black line) and modeled (dashed red line) EXAFS spectra (left) with the corresponding Fourier transforms (right) of all samples and reference compounds. Fit results are presented in Table 2.

Table 2. The spectra of all Fe samples differ from the reference compounds, especially at $k > 7$ Å^{-1}, implying that Am is structurally connected to a solid Fe phase and did not precipitate as $Am(OH)_3(s)$.

Reference Compounds. The EXAFS spectrum of $Am(III)_{aq}$ displays a single wave frequency of decreasing amplitude, consistent with the presence of only one ordered shell.

Accordingly, the FT exhibits only one peak located at $R + \Delta R$ = 2 Å. A good fit was obtained with one shell of 9.0(5) O atoms at R_{Am-O1} = 2.47(2) Å (Table 2), in agreement with earlier findings.[26,54] Compared to $Am(III)_{aq}$, the EXAFS spectrum of AmHydrox has lower wave frequency and amplitude maxima, hinting at a lower coordination number and a shorter interatomic distance for the first ligand shell. This is corroborated by the fit results yielding 5.7(10) O atoms at 2.39(2) Å. Higher distance contributions were observed on the FT, and modeled with ∼2 O at 3.36(6) Å and ∼2 Am at 3.76(6) Å. Critical assessment of these results is hampered by the absence of published interatomic distances and coordination numbers for Am neighboring shells in $Am(OH)_3(s)$. However, $Am(OH)_3(s)$[55] is isostructural with $Nd(OH)_3(s)$,[56] and both have comparable unit cell parameters (a = 6.426 Å and c = 3.745 Å for $Am(OH)_3(s)$ and a = 6.418 Å and c = 3.743 Å for $Nd(OH)_3(s)$), suggesting that $Nd(OH)_3(s)$ may be used as proxy for $Am(OH)_3(s)$. In $Nd(OH)_3(s)$, Nd is bound to two O subshells containing 3 and 6 atoms at 2.50 and 2.52 Å, respectively, and 2 Nd atoms are located at 3.74 Å. AmHydrox is poorly crystalline and thus EXAFS waves backscattered from neighboring atoms may partially damp out leading to a detected number of neighboring atoms lower than in the bulk structure, which would explain the relatively low coordination number of 5.7(10) for the first shell. The detection of an Am shell at 3.76(6) Å in AmHydrox compares more with the Nd−Nd distance in $Nd(OH)_3(s)$. The detection of an Am shell at similar distance in the Fe (hydr)oxide samples will thus be diagnostic of the presence of polymers/hydrous precipitate.

Green Rust Samples. The spectra of AmCopGR and AmCopGRtrans are very similar in oscillation amplitude and frequency, hinting at very similar chemical environments (Figure 3). The corresponding FTs display peaks at $R + \Delta R$ ∼ 2 and ∼3 Å, with only a small additional contribution at $R + \Delta R$ ∼ 3.5 Å for AmCopGRtrans. For both samples, good fits to the first shell were obtained with about 6 O atoms at R_{Am-O1} = 2.43(1) Å (Table 2). A next nearest Fe shell was modeled considering ∼2 Fe atoms at ∼3.45 Å. This bond length is moderately larger than interatomic distances for neighboring octahedral Fe in sulfate GR (3.18 Å[57]) or in $Fe(OH)_2(s)$ (3.25 Å[58]). The increase in distance from R_{Fe-Fe} to R_{Am-Fe} (0.20 to 0.27 Å) parallels the increase in ionic radius from Fe(II) or Fe(III) to Am(III) (0.20 to 0.33 Å), suggesting that the Fe shell at ∼3.45 Å may be attributed to neighboring octahedral Fe surrounding Am substituting for Fe in GR (AmCopGR) or in $Fe(OH)_2(s)$ (AmCopGRtrans). Some Am(III) may also be retained at the surface of the solids, which would be consistent with the low number of modeled Fe1 atoms and the number of O1 atoms slightly larger than six expected for Am located in an octahedral environment. No neighboring Am was detected, ruling out the presence of $Am(OH)_3(s)$ in the GR samples. In addition, the similarity of the EXAFS data for both GR samples with that for AmCopMag supports the possible incorporation of Am within magnetite particles present in AmCopGRtrans.

Magnetite Samples. The spectra of AmCopMag and AmAdsMag exhibit similar features, such as the high amplitude oscillation at k ∼ 6.5 $Å^{-1}$, but the oscillation amplitudes slightly differ at k > 8 $Å^{-1}$ (Figure 3). The spectrum of AmCopMagAged mainly differs from the two other magnetite samples by the lower amplitude oscillations (especially at k ∼ 7 $Å^{-1}$). The FT of AmCopMag and AmAdsMag both exhibit peaks at ∼2 and ∼3 Å, but the peak amplitudes are lower in AmCopMag. The FT maxima of AmCopMagAged have even lower amplitudes, and the peak near ∼2 Å is shifted to slightly shorter distance compared to the other magnetite samples. The FT of AmCopMagAged also contains a broad peak centered at ∼4 Å, and such a broad peak is absent in the FT of AmCopMag and AmAdsMag. These differences suggest that the Am(III) environment was modified either because of aging or of distinct synthesis conditions.

A good fit to the AmCopMag EXAFS data was provided considering a first shell of 7.1(5) O at R_{Am-O1} = 2.44(1) Å and higher distances shells of 3.7(7) Fe at R_{Am-Fe1} = 3.45(2) Å and 1.6(5) Fe at R_{Am-Fe2} = 3.98(5) Å (Table 2). The interatomic distances from Am to the O1 and Fe1 shells are similar to that in the GR samples, suggesting similar chemical environments in both samples. However, the O1 shell has a coordination number higher than expected for an octahedral environment (i.e., six atoms). Also, R_{Am-Fe1} = 3.45(2) Å is significantly larger than the interatomic distance for octahedral Fe (R_{Fe-Fe} = 2.97 Å,[59]) but close to the reported distance from octahedral Fe to tetrahedral Fe (R_{Fe-Fe} = 3.48 Å) in magnetite. Substitution of Am(III) for octahedral Fe(III) within bulk magnetite would result in the actinide being located at highly distorted sites. For such a species the number of modeled O atoms should be less than six because of damping out of EXAFS waves, in contrast to observations. Consequently, the data can best be explained by Am(III) taken up by magnetite at Fe(III) structural site at or near the surface, where the bonding environments might be less constrained. In that configuration some O atoms belong to magnetite and some others to bound OH^-/H_2O. This would be consistent with the rather high coordination number and interatomic distance of the O1 shell, as well as with Am and Fe polyhedra sharing corners with Am−O−Fe bond geometries ranging from bent (R_{Am-Fe1} = 3.45(2) Å) to close to linear (R_{Am-Fe2} = 3.98(5) Å). The Am retention is also associated with high structural strain, as attested by the relatively high mean square displacements (σ^2 = 0.008(2) $Å^2$) of both Fe shells. The O1 shell in AmCopMag is at shorter distance and contains fewer atoms compared to AmAdsMag (see below), ruling out compelling surface adsorption of the actinide onto magnetite in the coprecipitation sample. Finally, no neighboring Am could be detected, thus ruling out the formation of surface precipitate. The formation of such compounds is also unlikely based on reported hydrolysis constants of Am(III) hydrolysis species.[60]

The Am short range environment evolved upon aging, as shown by the decrease in R_{Am-O1} and N_{O1}. Compared to AmCopMag, the O1 and Fe1 shells in the aged sample are more consistent with an octahedral environment despite the low coordination numbers. Another evolution with aging is the increase in amplitude of FT contributions at $R + \Delta R$ > 3.5 Å, suggesting long range ordering appearing with sample aging. The data hint at a structural reorganization, especially around Am(III) centers, and thus an increase in structural order. This improved ordering resulted in constructive interferences of waves backscattered and thus the detection of atomic shells in AmCopMagAged. However, these contributions could not be fit because of the limited signal to noise ratio. The initial Am(III) incorporation does not result in the most stable local coordination environment, but this is improved with aging. This dynamic reorganization would in fact be consistent with the high reactivity of magnetite in Fe(II) containing aqueous environments (e.g.,[61]). No neighboring Am(III) was detected meaning that only marginal amount of actinide was released from the solid sample.

In AmAdsMag the Am(III) first shell consists of 8.8(5) O atoms at R_{Am-O1} = 2.48(1) Å, and next nearest neighboring shell is made of 5.5(7) Fe located at R_{Am-Fe1} = 3.50(2) Å (Table 2). No Am backscatterer was detected ruling out the presence of surface precipitate or Am(III) polymeric species. The O1 shell is similar to that in the reference $Am(III)_{aq}$, and thus not compatible with incorporation within the bulk structure. The data thus probably indicate an uptake of Am(III) at the surface upon contact with preformed magnetite in suspension.

The surface complex formed in AmAdsMag differs from that recently observed at pH 9.7,[26] and can be explained by contrasting chemical conditions, that is, pH and $[Fe]_f$. For example, hydrolysis increases with pH implying that a larger number of hydroxyl groups may bind Am(III) at pH 9.7 (in the previous study) than at pH 5.7 (for AmAdsMag). These differences can easily account for the detection of two O shells under slightly alkaline conditions in contrast to one shell in AmAdsMag. Another difference between the two studies is the number of fitted Fe neighbors at ∼3.5 Å. From structural considerations, Am can bind to a maximum of three Fe from the magnetite surface,[26] meaning that two additional Fe from the solution or possibly from moderate surface reorganization have to be considered to explain the high number of Fe neighbors for AmAdsMag. Interestingly, sample AmAdsMag in this study has a higher $[Fe]_f$ and a higher number of modeled Fe neighbors than in the reported study under more alkaline conditions. Fe(II) is 6 fold coordinated in solution and can adsorb at the magnetite surface, so that cosorption of this species around Am(III) would increase the number of fitted Fe backscatterers. In that configuration, the neighboring Fe shell would be made of Fe atoms from the magnetite surface together with cosorbed Fe atoms. Except the Fe(II) cosorption at the surface, the Am(III) surface complex in AmAdsMag is similar to that reported for Pu(III) adsorbed onto magnetite.[25]

■ DISCUSSION

The nature of the precipitates obtained by increasing the pH of a solution containing $Fe(II)_{aq}$ and $Fe(III)_{aq}$ depends on various factors such as pH and Fe(II):Fe(III) ratio.[52] Often ferrihydrite forms first and transforms quickly as a result of interfacial electron transfer from adsorbed Fe(II) and electron migration in the solid (e.g., refs 62 and 63). Proposed transformation mechanisms include ferrihydrite destabilization from electron hopping, resulting in dissolution reprecipitation (e.g., ref 64), and for magnetite, solid state transformation as well as dissolution reprecipitation (e.g., refs 63 and 65). The growth of these phases has been suggested to occur through dissolution reprecipitation (e.g., refs 63 and 66) or oriented attachment[67,68]. Recent cryo TEM studies indicate that coprecipitation from dissolved $Fe(II)_{aq}$ and $Fe(III)_{aq}$ also results in ferrihydrite, whose interaction with Fe(II) results in a ∼2 nm Fe(II) bearing Fe (hydr)oxide intermediate that upon oriented attachment produces magnetite. Finally, magnetite interaction with aqueous Fe(II) can result in isotope exchange and reequilibration of trace components, possibly correlated with recrystallization.[61] The presence of Am(III) during such reactions opens the possibility for uptake of the actinide by structural entrapment and/or surface adsorption.

Green Rust Samples and Fate of Trivalent Actinide. In the GR experiment, the Am concentration is too low to significantly influence the coprecipitation, but the increase in size from Fe(III) to Am(III) may nevertheless strongly impact the local Am(III) stability and thus the retention mode. According to the synthesis pathway, Am(III) was first retained by a poorly ordered ferric phase (either by surface adsorption and/or by structural incorporation) and subsequently by GR. EXAFS data indicate that the large Am(III) can substitute for Fe(III) within the GR octahedral sheet (sample AmCopGR) with, however, large distortion of the octahedral lattice site with a possible coordination of an extra O shell. The homovalent substitution seems to be possible to a limited extent, and this is certainly facilitated by the net charge balance. Steric hindrance seems to have little effect, probably because the GR brucite like structure is made of stacked octahedral sheets, which are likely to be able to accommodate the large actinide. This finding corroborates recent studies of Am substitution for Mg within brucite by direct precipitation.[45] A possible mechanism for Am(III) accommodation in the GR structure is a shift in the actinide position from the center of the octahedral site.

In a next step, increasing the pH of the AmCopGR suspension transformed GR into $Fe(OH)_2(s)$ and Fe_3O_4, in agreement with earlier studies.[52] Thus, the presence of the actinide did not affect the transformation pathway. During sample transformation, no detectable amounts of Am were released from the bulk structure and the chemical environment hardly changed, suggesting that Am(III) was still in an Fe octahedral sheet. This is consistent with Am(III) retention in the $Fe(OH)_2(s)$ octahedral layer, rather than at octahedral sites of magnetite. This formation pathway thus appears unfavorable for the incorporation of trivalent actinide within magnetite.

Magnetite Samples and (Geo)chemical Behavior of Americium. In the magnetite experiment, the presence of Am(III) also had no detectable influence on the coprecipitation, and XAS data suggests that Am substitutes for Fe in AmCopMag. Furthermore, comparing the data of AmCopMag to that of AmCopGRtrans indicates that the magnetite fraction in the transformation sample does not contain significant amounts of Am(III), and that most Am(III) stays in the remaining, more abundant $Fe(OH)_2(s)$. This finding indicates that the synthesis pathway plays a critical role in the actinide incorporation within magnetite, that is, that concomitantly forming $Fe(OH)_2$ will dominantly scavenge Am(III).

After aging for about two years, Am(III) is still located within magnetite in AmCopMagAged, but its crystallochemical environment was modified. The slight shortening in R_{Am-O1} confirms the octahedral coordination, and, compared to the AmAdsMag data, any Am release followed by surface adsorption on the solid can be ruled out. The Fe1 shell in the aged sample is also located at slightly shorter distance than in AmCopMag, and the interatomic distance is consistent with edge sharing between Fe and Am octahedra. The detection of higher distance shells in the aged sample further suggests an increased medium range order and corroborates a structural reorganization around Am(III) centers. Alternatively, the data could indicate that Am is located in a new phase. However, because magnetite is the most stable phase under the given chemical conditions, the entrapment of Am(III) into any other phase seems unlikely.

Consequences for the Fate of Actinides during Canister Corrosion. This study shows possible retention of the trivalent actinide, americium, within structures of Fe(II/III) (hydr)oxides or at the surfaces of these solids. This result is of importance in a nuclear waste repository system because all RN leached from the HLW are likely to be reduced into lower oxidation state(s) due to the ubiquity of steel and the H_2

evolution upon corrosion. The chemical conditions expected to develop in a repository would favor the formation of corrosion products such as $Fe(OH)_2(s)$, green rust and magnetite. Both $Fe(OH)_2(s)$ and GR show high affinity for Am(III), indicating that early stage anaerobic corrosion products could limit Am(III) mobility. Magnetite exhibits high reactivity in suspension in the presence of Fe(II),[61] and thus the binding mode of Am(III) retained by magnetite is likely to evolve. Initially, Am(III) can form surface sorbed species together with Fe(II) species in equilibrium with corrosion products. Surface dynamics, favored by the presence of dissolved Fe(II), can lead to Am(III) scavenged within the solid structure. Such an uptake sequence would explain the stable structural retention of Am(III) by magnetite over two years of contact time observed in the present study. Magnetite thus appears as a potential sink for RN, including Am, limiting their migration to the far field. Additional experiments investigating the effect of ligand(s) present in groundwater (e.g., carbonates), may be needed to enhance our understanding of uptake under real underground conditions.

■ AUTHOR INFORMATION

Corresponding Author

*Phone: +49 (0) 721 6082 4321; fax: +49 (0) 721 6082 3927; e mail: nicolas.finck@kit.edu.

Present Address

[‖]Haldor Topsøe A/S, Nymøllevej 55, 2800 Kgs. Lyngby, Denmark.

Author Contributions

The manuscript was written through contributions of all authors. All authors have given approval to the final version of the manuscript.

Notes

The authors declare no competing financial interest.

■ ACKNOWLEDGMENTS

We thank E. Soballa (KIT INE) for SEM analysis, M. Lagos and F. Geyer (KIT INE) for ICP MS measurements, F. Huber (KIT INE) for help in the laboratory, the radioprotection officers for assistance and K. Dardennne (KIT INE) for help at the INE Beamline. The synchrotron light source ANKA is acknowledged for providing beamtime. This work has been supported by the European FP7 TALSIMAN (Transnational Access to Large Infrastructure for a Safe Management of ActiNides) project grant agreement #323300, JRP no TALI C01 13.

■ REFERENCES

(1) Bennett, D. G.; Gens, R. Overview of European concepts for high level waste and spent fuel disposal with special reference waste container corrosion. *J. Nucl. Mater.* **2008**, *379* (1−3), 1−8.

(2) Martin, F. A.; Bataillon, C.; Schlegel, M. L. Corrosion of iron and low alloyed steel within a water saturated brick of clay under anaerobic deep geological disposal conditions: An integrated experiment. *J. Nucl. Mater.* **2008**, *379* (1−3), 80−90.

(3) Pignatelli, I.; Bourdelle, F.; Bartier, D.; Mosser Ruck, R.; Truche, L.; Mugnaioli, E.; Michau, N. Iron−clay interactions: Detailed study of the mineralogical transformation of claystone with emphasis on the formation of iron rich T−O phyllosilicates in a step by step cooling experiment from 90 to 40 °C. *Chem. Geol.* **2014**, *387* (1), 1−11.

(4) Schlegel, M. L.; Bataillon, C.; Brucker, F.; Blanc, C.; Prêt, D.; Foy, E.; Chorro, M. Corrosion of metal iron in contact with anoxic clay at 90 °C: Characterization of the corrosion products after two years of interaction. *Appl. Geochem.* **2014**, *51* (1), 1−14.

(5) Schlegel, M. L.; Bataillon, C.; Blanc, C.; Prêt, D.; Foy, E. Anodic activation of iron corrosion in clay media under water saturated conditions at 90 °C: Characterization of the corrosion interface. *Environ. Sci. Technol.* **2010**, *44* (4), 1503−1508.

(6) Schlegel, M. L.; Bataillon, C.; Benhamida, K.; Blanc, C.; Menut, D.; Lacour, J. L. Metal corrosion and argillite transformation at the water saturated, high temperature iron−clay interface: A microscopic scale study. *Appl. Geochem.* **2008**, *23* (9), 2619−2633.

(7) Burger, E.; Rebiscoul, D.; Bruguier, F.; Jublot, M.; Lartigue, J. E.; Gin, S. Impact of iron on nuclear glass alteration in geological repository conditions: A multiscale approach. *Appl. Geochem.* **2013**, *31* (1), 159−170.

(8) de Combarieu, G.; Schlegel, M. L.; Neff, D.; Foy, E.; Vantelon, D.; Barboux, P.; Gin, S. Glass−iron−clay interactions in a radioactive waste geological disposal: An integrated laboratory scale experiment. *Appl. Geochem.* **2011**, *26* (1), 65−79.

(9) Ferriss, E. D. A.; Helean, K. B.; Bryan, C. R.; Brady, P. V.; Ewing, R. C. UO_2 corrosion in an iron waste package. *J. Nucl. Mater.* **2009**, *384* (2), 130−139.

(10) Schlegel, M. L.; Necib, S.; Daumas, S.; Blanc, C.; Foy, E.; Trcera, N.; Romaine, A. Microstructural characterization of carbon steel corrosion in clay borehole water under anoxic and transient acidic conditions. *Corros. Sci.* **2016**, *109* (1), 126−144.

(11) Schikorr, G. Über Eisen(II) hydroxyd und ein ferromagne tisches Eisen(III) hydroxyd. *Z. Anorg. Allg. Chem.* **1933**, *212* (1), 33−39.

(12) Refait, P. H.; Abdelmoula, M.; Génin, J. M. R. Mechanisms of formation and structure of green rust one in aqueous corrosion of iron in the presence of chloride ions. *Corros. Sci.* **1998**, *40* (9), 1547−1560.

(13) Pineau, S.; Sabot, R.; Quillet, L.; Jeannin, M.; Caplat, C.; Dupont Morral, I.; Refait, P. Formation of the Fe(II−III) hydroxysulphate green rust during marine corrosion of steel associated to molecular detection of dissimilatory sulphite reductase. *Corros. Sci.* **2008**, *50* (4), 1099−1111.

(14) Génin, J. M. R.; Olowe, A. A.; Resiak, B.; Confente, M.; Rollet Benbouzid, N.; L'Haridon, S.; Prieur, D. Products obtained by microbially induced corrosion of steel in a marine environment: Role of green rust two. *Hyperfine Interact.* **1994**, *93* (1), 1807−1812.

(15) Kim, J. I.; Grambow, B. Geochemical assessement of actinide isolation in a German salt repository environment. *Eng. Geol.* **1999**, *52* (3−4), 221−230.

(16) Upadhyay, R. V.; Gupta, A.; Sudakar, C.; Rao, K. V.; Parekh, K.; Desai, R.; Mehta, R. V. Effect of rare earth Ho ion substitution on magnetic properties of Fe_3O_4 magnetic fluids. *J. Appl. Phys.* **2006**, *99* (8), 08M906.

(17) De Silva, C. R.; Smith, S.; Shim, I.; Pyun, J.; Gutu, T.; Jiao, J.; Zheng, Z. P. Lanthanide(III) doped magnetite nanoparticles. *J. Am. Chem. Soc.* **2009**, *131* (18), 6336−6337.

(18) Rice, K. P.; Russek, S. E.; Geiss, R. H.; Shaw, J. M.; Usselman, R. J.; Evarts, E. R.; Silva, T. J.; Nembach, H. T.; Arenholz, E.; Idzerda, Y. U. Temperature dependent structure of Tb doped magnetite nano particles. *Appl. Phys. Lett.* **2015**, *106* (6), 062409.

(19) Moon, J. W.; Yeary, L. W.; Rondinone, A. J.; Rawn, C. J.; Kirkham, M. J.; Roh, Y.; Love, L. J.; Phelps, T. J. Magnetic response of microbially synthesized transition metal and lanthanide substituted nano sized magnetites. *J. Magn. Magn. Mater.* **2007**, *313* (2), 283−292.

(20) Nedel, S.; Dideriksen, K.; Christiansen, B. C.; Bovet, N.; Stipp, S. L. S. Uptake and release of cerium during Fe oxide formation and transformation in Fe(II) solutions. *Environ. Sci. Technol.* **2010**, *44* (12), 4493−4498.

(21) Carvalho, R. S.; Daniel da Silva, A. L.; Trindade, T. Uptake of europium(III) from water using magnetite nanoparticles. *Part. Part. Syst. Charact.* **2016**, *33* (3), 150−157.

(22) Catalette, H.; Dumonceau, J.; Ollar, P. Sorption of cesium, barium and europium on magnetite. *J. Contam. Hydrol.* **1998**, *35* (1−3), 151−159.

(23) Marmier, N.; Delisée, A.; Fromage, F. Surface complexation modeling of Yb(III), Ni(II), and Cs(I) sorption on magnetite. *J. Colloid Interface Sci.* **1999**, *211* (1), 54−60.

(24) Tsukamoto, M.; Fujita, T.; Christensen, H. Sorption of actinides on magnetite and goethite under reducing conditions. *Czech. J. Phys.* **2006**, *56* (Suppl.D), D339−D348.

(25) Kirsch, R.; Fellhauer, D.; Altmaier, M.; Neck, V.; Rossberg, A.; Fanghänel, T.; Charlet, L.; Scheinost, A. C. Oxidation state and local structure of plutonium reacted with magnetite, mackinawite and chukanovite. *Environ. Sci. Technol.* **2011**, *45* (17), 7267−7274.

(26) Finck, N.; Radulescu, L.; Schild, D.; Rothmeier, M.; Huber, F.; Lützenkirchen, J.; Rabung, T.; Heberling, F.; Schlegel, M. L.; Dideriksen, K.; Nedel, S.; Geckeis, H. XAS signatures of Am(III) adsorbed onto magnetite and maghemite. *J. Phys.: Conf. Ser.* **2016**, *712* (1), 012085.

(27) Seco, F.; Hennig, C.; Pablo, J. d.; Rovira, M.; Rojo, I.; Martí, V.; Giménez, J.; Duro, L.; Grivé, M.; Bruno, J. Sorption of Th(IV) onto iron corrosion products: EXAFS study. *Environ. Sci. Technol.* **2009**, *43* (8), 2825−2830.

(28) Marshall, T. A.; Morris, K.; Law, G. T. W.; Mosselmans, J. F. W.; Bots, P.; Roberts, H.; Shaw, S. Uranium fate during crystallization of magnetite from ferrihydrite in conditions relevant to the disposal of radioactive waste. *Mineral. Mag.* **2015**, *79* (6), 1265−1274.

(29) Marshall, T. A.; Morris, K.; Law, G. T. W.; Mosselmans, J. F. W.; Bots, P.; Parry, S. A.; Shaw, S. Incorporation and retention of 99 Tc(IV) in magnetite under high pH conditions. *Environ. Sci. Technol.* **2014**, *48* (20), 11853−11862.

(30) Missana, T.; Maffiotte, C.; García Gutiérrez, M. Surface reactions kinetics between nanocrystalline magnetite and uranyl. *J. Colloid Interface Sci.* **2003**, *261* (1), 154−160.

(31) Scott, T. B.; Allen, G. C.; Heard, P. J.; Randell, M. G. Reduction of U(VI) to U(IV) on the surface of magnetite. *Geochim. Cosmochim. Acta* **2005**, *69* (24), 5639−5646.

(32) Ilton, E. S.; Boily, J. F.; Buck, E. C.; Skomurski, F. N.; Rosso, K. M.; Cahill, C. L.; Bargar, J. R.; Felmy, A. R. Influence of dynamical conditions on the reduction of U(VI) at the magnetite−solution interface. *Environ. Sci. Technol.* **2010**, *44* (1), 170−176.

(33) Latta, D. E.; Gorski, C. A.; Boyanov, M. I.; O'Loughlin, E. J.; Kemner, K. M.; Scherer, M. M. Influence of magnetite stoichiometry on U(VI) reduction. *Environ. Sci. Technol.* **2012**, *46* (2), 778−786.

(34) Huber, F.; Schild, D.; Vitova, T.; Rothe, J.; Kirsch, R.; Schäfer, T. U(VI) removal kinetics in presence of synthetic magnetite nanoparticles. *Geochim. Cosmochim. Acta* **2012**, *96* (1), 154−173.

(35) Singer, D. M.; Chatman, S. M.; Ilton, E. S.; Rosso, K. M.; Banfield, J. F.; Waychunas, G. A. Identification of simultaneous U(VI) sorption complexes and U(IV) nanoprecipitates on the magnetite (111) surface. *Environ. Sci. Technol.* **2012**, *46* (7), 3811−3820.

(36) Nakata, K.; Nagasaki, S.; Tanaka, S.; Sakamoto, Y.; Tanaka, T.; Ogawa, H. Sorption and reduction of neptunium(V) on the surface of iron oxides. *Radiochim. Acta* **2002**, *90* (9−11), 665−669.

(37) Nakata, K.; Nagasaki, S.; Tanaka, S.; Sakamoto, Y.; Tanaka, T.; Ogawa, H. Reduction rate of neptunium(V) in heterogeneous solution with magnetite. *Radiochim. Acta* **2004**, *92* (3), 145−149.

(38) Powell, B. A.; Fjeld, R. A.; Kaplan, D. I.; Coates, J. T.; Serkiz, S. M. $Pu(V)O_2^+$ adsorption and reduction by synthetic magnetite (Fe_3O_4). *Environ. Sci. Technol.* **2004**, *38* (22), 6016−6024.

(39) Pepper, S. E.; Bunker, D. J.; Bryan, N. D.; Livens, F. R.; Charnock, J. M.; Pattrick, R. A. D.; Collison, D. Treatment of radioactive wastes: An X ray absorption spectroscopy study of the reaction of technetium with green rust. *J. Colloid Interface Sci.* **2003**, *268* (2), 408−412.

(40) O'Loughlin, E. J.; Kelly, S. D.; Cook, R. E.; Csencsits, R.; Kemner, K. M. Reduction of uranium(VI) by mixed iron(II)/iron(III) hydroxide (green rust): Formation of UO_2 nanoparticles. *Environ. Sci. Technol.* **2003**, *37* (4), 721−727.

(41) Latta, D. E.; Boyanov, M. I.; Kemner, K. M.; O'Loughlin, E. J.; Scherer, M. M. Reaction of uranium(VI) with green rusts: Effect of interlayer anion. *Curr. Inorg. Chem.* **2015**, *5* (3), 156−168.

(42) Christiansen, B. C.; Geckeis, H.; Marquardt, C. M.; Bauer, A.; Römer, J.; Wiss, T.; Schild, D.; Stipp, S. L. S. Neptunyl (Np) interaction with green rust. *Geochim. Cosmochim. Acta* **2011**, *75* (5), 1216−1226.

(43) Bach, D.; Christiansen, B. C.; Schild, D.; Geckeis, H. TEM study of green rust sodium sulphate ($GR_{Na,SO4}$) interacted with neptunyl ions (NpO_2^+). *Radiochim. Acta* **2014**, *102* (4), 279−289.

(44) Shannon, R. D. Revised effective ionic radii and systematic studies of interatomic distances in halides and chalcogenides. *Acta Crystallogr., Sect. A: Cryst. Phys., Diffr., Theor. Gen. Crystallogr.* **1976**, *32* (5), 751−767.

(45) Finck, N.; Dardenne, K.; Geckeis, H. Am(III) coprecipitation with and adsorption on the smectite hectorite. *Chem. Geol.* **2015**, *409* (1), 12−19.

(46) Stumpf, T.; Marques Fernandes, M.; Walther, C.; Dardenne, K.; Fanghänel, T. Structural characterization of Am incorporated into calcite: A TRLFS and EXAFS study. *J. Colloid Interface Sci.* **2006**, *302* (1), 240−245.

(47) Rothe, J.; Butorin, S.; Dardenne, K.; Denecke, M. A.; Kienzler, B.; Loble, M.; Metz, V.; Seibert, A.; Steppert, M.; Vitova, T.; Walther, C.; Geckeis, H. The INE Beamline for actinide science at ANKA. *Rev. Sci. Instrum.* **2012**, *83* (4), 043105.

(48) Brendebach, B.; Banik, N. L.; Marquardt, C. M.; Rothe, J.; Denecke, M. A.; Geckeis, H. X ray absorption spectroscopic study of trivalent and tetravalent actinides in solution at varying pH values. *Radiochim. Acta* **2009**, *97* (12), 701−708.

(49) Ravel, B.; Newville, M. ATHENA, ARTEMIS, HEPHAESTUS: data analysis for X ray absorption spectroscopy using IFEFFIT. *J. Synchrotron Radiat.* **2005**, *12* (4), 537−541.

(50) Ankudinov, A. L.; Ravel, B.; Rehr, J. J.; Conradson, S. D. Real space multiple scattering calculation and interpretation of x ray absorption near edge structure. *Phys. Rev. B: Condens. Matter Mater. Phys.* **1998**, *58* (12), 7565−7576.

(51) Feitknecht, W.; Keller, G. Über Die dunkelgrünen Hydroxyverbindungen des Eisens. *Z. Anorg. Chem.* **1950**, *262* (1−5), 61−68.

(52) Jolivet, J. P.; Tronc, E.; Chanéac, C. Iron oxides: From molecular clusters to solid. A nice example of chemical versatility. *C. R. Geosci.* **2006**, *338* (6−7), 488−497.

(53) Jolivet, J. P.; Tronc, E. Interfacial electron transfer in colloidal spinel iron oxide. Conversion of Fe_3O_4 γFe_2O_3 in aqueous medium. *J. Colloid Interface Sci.* **1988**, *125* (2), 688−701.

(54) Skerencak Frech, A.; Fröhlich, D. R.; Rothe, J.; Dardenne, K.; Panak, P. J. Combined time resolved laser fluorescence spectroscopy and extended X ray absorption fine structure spectroscopy study on the complexation of trivalent actinides with chloride at T = 25−200 °C. *Inorg. Chem.* **2014**, *53* (2), 1062−1069.

(55) Milligan, W. O.; Beasley, M. L.; Lloyd, M. H.; Haire, R. G. Crystalline americium trihydroxide. *Acta Crystallogr., Sect. B: Struct. Crystallogr. Cryst. Chem.* **1968**, *24* (7), 979−980.

(56) Beall, G. W.; Milligan, W. O.; Dillin, D. R.; Williams, R. J.; McCoy, J. J. Refinement of neodymium trihydroxide. *Acta Crystallogr., Sect. B: Struct. Crystallogr. Cryst. Chem.* **1976**, *32* (7), 2227−2229.

(57) Simon, L.; François, M.; Refait, P.; Renaudin, G.; Lelaurain, M.; Génin, J. M. R. Structure of the Fe(II III) layered double hydroxysulphate green rust two from Rietveld analysis. *Solid State Sci.* **2003**, *5* (2), 327−334.

(58) Natta, G. Costituzione degli idrossidi ed idrati. Nota I. *Gazz. Chim. Ital.* **1928**, *58*, 344−358.

(59) Fleet, M. E. The structure of magnetite: Symmetry of cubic spinels. *J. Solid State Chem.* **1986**, *62* (1), 75−82.

(60) Guillaumont, R.; Fanghänel, T.; Fuger, J.; Grenthe, I.; Neck, V.; Palmer, D. A.; Rand, M. H. *Update on the Chemical Thermodynamics of Uranium, Neptunium, Plutonium, Americium and Technetium*; Elsevier, B. V.: Amsterdam, The Nederlands, 2003.

(61) Gorski, C. A.; Handler, R. M.; Beard, B. L.; Pasakarnis, T.; Johnson, C. M.; Scherer, M. M. Fe atom exchange between aqueous Fe^{2+} and magnetite. *Environ. Sci. Technol.* **2012**, *46* (22), 12399−12407.

(62) Williams, A. G. B.; Scherer, M. M. Spectroscopic evidence for Fe(II)−Fe(III) electron transfer at the iron oxide−water interface. *Environ. Sci. Technol.* **2004**, *38* (18), 4782−4790.
(63) Tronc, E.; Belleville, P.; Jolivet, J. P.; Livage, J. Transformation of ferric hydroxide into spinel by iron(II) adsorption. *Langmuir* **1992**, *8* (1), 313−319.
(64) Pedersen, H. D.; Postma, D.; Jakobsen, R.; Larsen, O. Fast transformation of iron oxyhydroxides by the catalytic action of aqueous Fe(II). *Geochim. Cosmochim. Acta* **2005**, *69* (16), 3967−3977.
(65) Yang, L.; Steefel, C. I.; Marcus, M. A.; Bargar, J. R. Kinetics of Fe(II) catalyzed transformation of 6 line ferrihydrite under anaerobic flow conditions. *Environ. Sci. Technol.* **2010**, *44* (14), 5469−5475.
(66) Guilbaud, R.; White, M. L.; Poulton, S. W. Surface charge and growth of sulphate and carbonate green rust in aqueous media. *Geochim. Cosmochim. Acta* **2013**, *108* (1), 141−153.
(67) Baumgartner, J.; Dey, A.; Bomans, P. H. H.; Le Coadou, C.; Fratzl, P.; Sommerdijk, N. A. J. M.; Faivre, D. Nucleation and growth of magnetite from solution. *Nat. Mater.* **2013**, *12* (4), 310−314.
(68) Johnson, C. A.; Murayama, M.; Kusel, K.; Hochella, M. F. Polycrystallinity of green rust minerals and their synthetic analogs: Implications for particle formation and reactivity in complex systems. *Am. Mineral.* **2015**, *100* (10), 2091−2105.